Stochastic resonant damping in a noisy monostable system: Theory and experiment

Giovanni Volpe,[1] Sandro Perrone,[1] J. Miguel Rubi,[2] and Dmitri Petrov[1,3]
[1]*ICFO–Institut de Ciències Fotóniques, Mediterranean Technology Park, 08860, Castelldefels, Barcelona, Spain*
[2]*Departament de Física Fonamental, Universitat de Barcelona, Diagonal 647, 08028 Barcelona, Spain*
[3]*ICREA–Institució Catalana de Recerca i Estudis Avançats, 08010, Barcelona, Spain*
(Received 14 February 2008; revised manuscript received 25 March 2008; published 9 May 2008)

Usually in the presence of a background noise an increased effort put in controlling a system stabilizes its behavior. Rarely it is thought that an increased control of the system can lead to a looser response and, therefore, to a poorer performance. Strikingly there are many systems that show this weird behavior; examples can be drawn form physical, biological, and social systems. Until now no simple and general mechanism underlying such behaviors has been identified. Here we show that such a mechanism, named *stochastic resonant damping*, can be provided by the interplay between the background noise and the control exerted on the system. We experimentally verify our prediction on a physical model system based on a colloidal particle held in an oscillating optical potential. Our result adds a tool for the study of intrinsically noisy phenomena, joining the many constructive facets of noise identified in the past decades—for example, stochastic resonance, noise-induced activation, and Brownian ratchets.

DOI: 10.1103/PhysRevE.77.051107 PACS number(s): 05.40.−a, 02.50.−r

I. INTRODUCTION

The presence of noise is ubiquitous in natural, social, and technological phenomena, ranging from nanoscopic systems such as biomolecules and nanodevices to macroscopic systems such as financial markets and human organizations. Noise introduces disorder and random fluctuations into any type of system; and often this is deleterious for the system performance.

In recent years considerable and increasing attention has been focused on the constructive role of noise in nature: the influence of noise is not restricted to destructive and thermodynamic effects, but can have positive outcomes. Examples include stochastic resonance [1], in which the addition of noise to an input signal improves the output signal-to-noise ratio (SNR); Brownian ratchets and motors [2], in which the thermal jiggling of a Brownian particle can be rectified by a periodic asymmetric or oscillating potential; and noise-induced activation [3,4], in which a minimal averaged residence time occurs at an optimal time scale of the modulation of a potential barrier.

Despite that, there are systems for which noise is still a nuisance. In these cases it is desirable to stabilize the system—i.e., to reduce its output noise. One straightforward way to achieve this is to increase the effort that confines the system near an equilibrium state and therefore reduces its *intrinsic noise*. However, for many systems the confinement parameters are noisy; i.e., the confinement process introduces a second noise (*parametric noise*) in the system. This is the case, in particular, of any nanoscopic system, such as a biomolecule or a nanodevice, since the role of thermal fluctuations in the confinement parameters cannot be neglected. For example, the mechanism of motor protein motion in the cytoskeleton has been successfully modeled by Brownian ratchets: the motor protein kinesin can be driven by the action of both the thermal noise and an additive colored noise, whose finite correlation time corresponds to the kinesin binding events and subsequent energy release through hydrolysis [2,5,6]. In [7] the interplay between an externally added noise and the intrinsic noise of systems that relax fast toward a stationary state was analyzed theoretically. It was found that increasing the intensity of the external noise can reduce the total noise of the system. The output noise reduction is due to the fact that the system is driven into states with lower intrinsic noise, where the confinement effort is effectively greater.

Here, we study theoretically and experimentally the situation when the confinement effort is increased at a fixed intrinsic and parametric noise level. Counterintuitively, we show that in most cases an increased confinement effort over a certain threshold leads to a poorer system performance. More specifically, we show that the minimum output variance is typically, but not always, achieved for a finite confinement effort, and therefore to increase the confinement effort over this threshold value leads to a poorer performance. This feature derives from the interplay between the *intrinsic noise*, whose characteristic frequency depends on the confinement effort, and the *parametric noise* of the confinement effort exerted on the system. We name this effect *stochastic resonant damping* because of its similarities to stochastic resonance; however, while stochastic resonance is concerned with the maximization of the SNR [1], stochastic resonant damping is concerned with the minimization of the system output variance. We use a mathematical model that is linear and exactly solvable, but the main characteristics are also observed under more arbitrary conditions. We experimentally verify our prediction on a physical model system based on a colloidal particle held in an oscillating optical trapping potential. We finally show how stochastic resonant damping can be useful for the study of phenomena in various fields.

II. MATHEMATICAL MODEL

We consider a system whose behavior can be described by the Langevin equation

$$\dot{x}(t) + C[x(t) - x_0(t)] = Dh(t). \quad (1)$$

The intrinsic noise is driven by a white Gaussian random process $h(t)$ such that $\langle h(t)\rangle = 0$ and $\langle h(t+\tau)h(t)\rangle = \delta(\tau)$; D determines the intensity of the noise. The system is constrained by the restoring term $C[x(t)-x_0(t)]$, whose equilibrium position $x_0(t)$ can vary over time either deterministically or randomly. The value C defines the confinement effort—i.e., a measure of the effort applied to the system for its confinement.

The choice of this model is motivated by the fact that it is exactly solvable and readily experimentally implementable. This permits us to directly compare theoretical and experimental results. As we will see in more detail in the experimental section, Eq. (1) describes an overdamped Brownian motion in the presence of an oscillating harmonic potential: $x(t)$ is the position of a Brownian particle with diffusion coefficient $D^2/2$ in the presence of a harmonic trapping potential characterized by a fixed stiffness proportional to C and an oscillating center $x_0(t)$. In the case this potential is generated by an optical trap, C is proportional to the optical trapping power and inversely proportional to the viscosity. In underdamped mechanical systems, such as the Brownian movement of atomics wave packets in magneto-optical traps, the trap modulation induces an increase in damping and a decrease of the spatial extension of the atomic wave packets [8,9]. Parametrical resonance in underdamped systems (optically trapped aerosols), which leads to a decrease of the output noise, was observed by periodical modulation of the trapping power in [10]. However, previous experiments performed in the overdamped regime [11] have only showed that the modulation of the trap power by a harmonic signal increases the variance of the colloidal particle motion. A decrease of the particle position variance was achieved in a modulated optical trap in [12], but at the expenses of a higher confinement effort.

We are interested in studying the output variance σ_x^2 of the system with modulation of the trap position as a function of C for a given $x_0(t)$, which can be either a deterministic or a stochastic function. Solving (1) in the Fourier domain leads to

$$X(f) = \frac{DH(f) + CX_0(f)}{C + i2\pi f}, \quad (2)$$

where $H(f)$, $X(f)$, and $X_0(f)$ are the Fourier transforms of $h(t)$, $x(t)$, and $x_0(t)$. In the absence of modulation—i.e., $x_0(t) \equiv 0$—the power spectral density (PSD) is $P_x(f) = \langle H(f)^\dagger H(f)\rangle = D^2/(C^2+4\pi^2 f^2)$, where the dagger represents complex conjugation. It describes the intrinsic system noise in the presence of a confinement potential and is characterized by the cutoff frequency $f_c = C/2\pi$.

Using Parseval's theorem the system output variance can be calculated as $\sigma_x^2 = \int_{-\infty}^{+\infty} \langle X(f)^\dagger X(f)\rangle df$ under the assumption that $\langle x(t)\rangle = 0$. Considering that $\langle H^\dagger H\rangle = 1$ and the intrinsic noise h and the modulation signal x_0 are uncorrelated—i.e., $\langle H^\dagger X_0\rangle = \langle X_0^\dagger H\rangle = 0$—we get

$$\sigma_x^2 = \frac{D^2}{2C} + \int_{-\infty}^{+\infty} \frac{C^2}{C^2 + 4\pi^2 f^2} \langle |X_0(f)|^2\rangle df, \quad (3)$$

where the first term represent the *intrinsic noise* contribution and the second term the *parametric noise* contribution. It follows straightforwardly that the total variance in the externally modulated system always exceeds the intrinsic noise. The output response depends on the power spectral density of x_0 describing the movement of the equilibrium position.

First we consider the case when $x_0(t)$ is a white Gaussian random process with $\langle |X_0(f)|^2\rangle = N^2$; then,

$$\sigma_x^2 = \frac{D^2 + N^2C^2}{2C}. \quad (4)$$

For increasing confinement effort C, the output variance initially decreases and then it increases. This behavior can be explained as follows: while the confinement effort C increases, the intrinsic noise cutoff frequency f_c increases as well and therefore more components of the parametric noise have a pronounced effect on the system. However, in this case the power of the noise is infinite, while in the real cases it is finite. In particular, the output variance in this case diverges for C, tending to infinity, while this never happens for real noises that do have a cutoff frequency. Therefore, in the following examples we will consider noises with finite variance.

In the case where the equilibrium position moves harmonically, $\langle |X_0(f)|^2\rangle = A^2[\frac{1}{2}\delta(f-f_0) + \frac{1}{2}\delta(f+f_0)]$ (notice that its variance is normalized to A^2) and

$$\sigma_x^2 = \frac{D^2}{2C} + A^2 \frac{C^2}{C^2 + 4\pi^2 f_0^2}. \quad (5)$$

In Fig. 1(a) the system variance σ_x^2 as a function of C and the forcing frequency f_0 is represented. The σ_x^2 diverges for vanishing C, because the confinement is lost. For very low forcing frequencies ($f_0 \ll \frac{C}{2\pi}$) as well as for high forcing frequencies ($f_0 \gg \frac{C}{2\pi}$), σ_x^2 monotonically decreases with increasing the confinement effort C. However, there is a range of frequencies f_0 when a minimum of the output variance can be achieved for a finite value of C.

This effect, which we name *stochastic resonant damping*, is similar to stochastic resonance. Both indeed are due to a pseudoresonance between the forcing frequency f_0 and a packet of frequencies from the range of intrinsic frequencies of the system noise whose cutoff is $f_c = C/2\pi$. The difference is that stochastic resonance is concerned with a maximum in the SNR, while stochastic resonant damping is concerned with a minimum of the output variance. Interestingly enough, the two phenomena may occur simultaneously in the same system, although typically in quite different parameter regimes; this should be the object of further studies. At a modulation frequency $f_0 = 1$ Hz the squeezing of the output variance is observed at $C=2$, corresponding to the intrinsic system noise cutoff frequency $f_c = 1/\pi$ Hz. Figure 2 illustrates the counterintuitive aspects of *stochastic resonant damping*: while the effort made to increase the confinement is increased, the system output variance first diminishes [comparison between Figs. 2(a) and 2(b)] and then starts growing again [comparison between Figs. 2(b) and 2(c)]. Hence, in this simple case of harmonic modulation of the equilibrium position the system reveals an unexpected be-

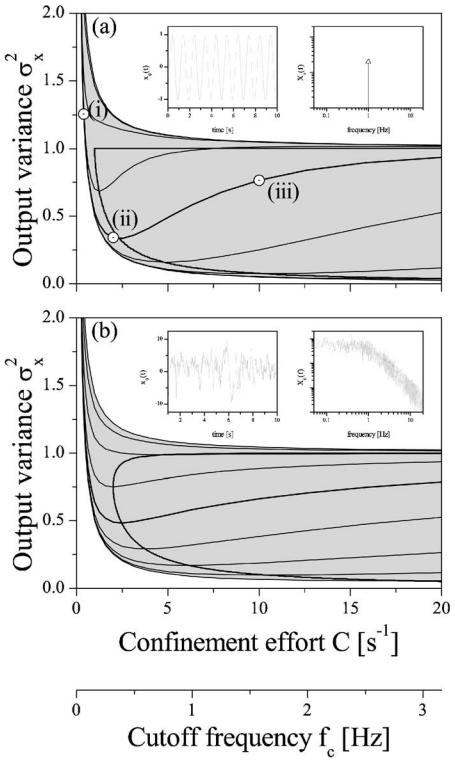

FIG. 1. Output system variance σ_x^2 as a function of the confinement effort C ($D=1$, $A=1$) for harmonic (a) and colored Gaussian (b) parametric noise for various values of the frequency f_0: from bottom to top $f_0=100$, 31, 10, 3, 1 (thick curve), 0.3, 0.1, 0.03, 0.01 Hz. The thick line indicates the σ_x^2 minima. The shaded area represents the range of accessible output variance for a given value of the confinement effort. The additional axis shows the system intrinsic noise cutoff frequency f_c. Insets: a typical example of x_0 in time and frequency domain ($f_0=1$).

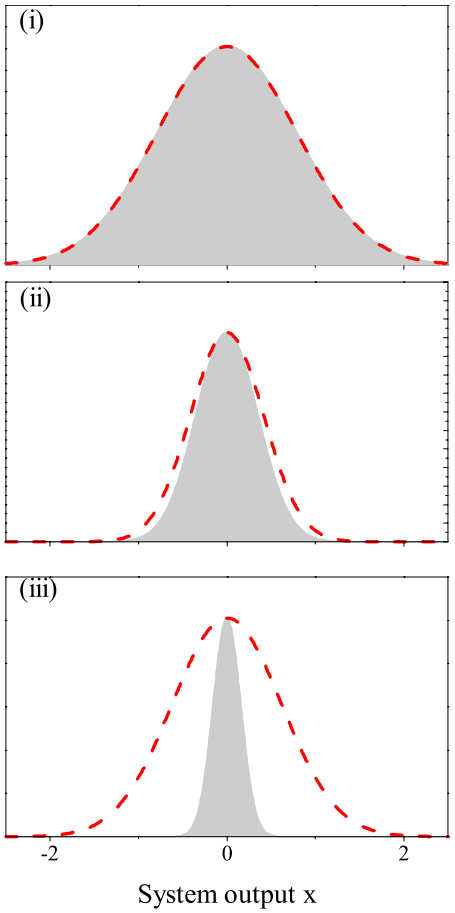

FIG. 2. (Color online) Intrinsic system output (gray filled area) and system output in the presence of a sinusoidal modulation ($f_0=1$, $D=1$, $A=1$) (red dashed curve) for three states of the system, indicated by dots in Fig. 1(a) for the modulation frequency $f_0=1Hz$: (i) $C=0.4$ ($f_c=0.064$ Hz), (ii) $C=2$ ($f_c=0.32$ Hz) corresponding to the absolute variance minimum, and (iii) $C=10$ ($f_c=1.6$ Hz). The output variance always exceeds the intrinsic variance.

havior: the more effort (over a certain threshold) is exerted to confine the system, the less confinement is achieved.

Noises occurring in nature are typically more complex than a harmonic modulation. Non-Markovian noise sources can be found in various biological systems [13], such as currents through voltage-sensitive ion channels in cell membranes and signals from the sensory system of rat skin [14–16]. Biological transport phenomena work in the presence of thermal noise and internal, generally correlated, random noise of biological origin, such as the hydrolysis mechanism Adenosine-Triphosphate [5]. It is therefore important to analyze also the movement of the equilibrium position of the system governed by a colored noise. We therefore consider the simplest case of a colored Gaussian forcing with PSD $\langle |X_0(f)|^2 \rangle = A^2 f_0 / \pi(f_0^2+f^2)$ (notice that its variance is again A^2 and f_0 is its characteristic frequency). The system variance is now

$$\sigma_x^2 = \frac{D^2}{2C} + A^2 \frac{C}{C+2\pi f_0}. \tag{6}$$

In Fig. 1(b) the system variance σ_x^2 as a function of C and the characteristic frequency f_0 is represented. The overall behavior is similar to the one presented in Fig. 1(a) for harmonic forcing. The value of the confinement effort C_{opt} which provides a minimal variance as a function of the characteristic frequency f_0 and the noise power A^2 of x_0 is

$$C_{opt} = \begin{cases} +\infty & \text{for } f_0 A^2 < D^2/4\pi, \\ 2\pi f_0 D/(2\sqrt{\pi f_0} A - D) & \text{for } f_0 A^2 \geq D^2/4\pi. \end{cases} \tag{7}$$

In Fig. 1(b) the thick curve shows the behavior of C_{opt}.

Until now we have only considered a noise of constant intensity—i.e., $A^2=$const. If we now explore how the output variance σ_x^2 varies as a function of the noise intensity A^2, the σ_x^2 increases with an increase of the noise intensity A^2. We found that the variance minima becomes deeper as the noise intensity grows. The depth of the variance minima can be defined as $\sigma_x^2(C_{opt})/\sigma_x^2(C=+\infty)$. Hence, the present result is more evident for highly noisy systems.

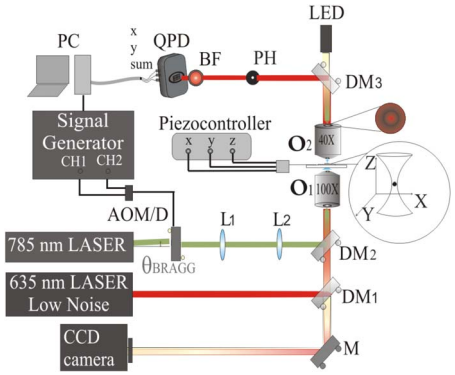

FIG. 3. (Color online) Experimental setup: O_1, 100× objective; O_2, 40× objective; DM_1, DM_2, and DM_3, dichroic mirrors; M, mirror; AOM/D, acousto-optic modulator/deflector; L_1 and L_2, optical system for conjugation of the output plane of the acousto-optical deflector and the entrance pupil of the objective O_1; PH, pinhole; BF, bandpass filter; QPD, quadrant photodetector.

III. EXPERIMENTAL VERIFICATION

As we anticipated above, a paradigmatic system that behaves according to the theory presented is a Brownian particle held in an oscillating trapping potential. We have therefore used such a physical system in order to verify our predictions. We implemented this system using an optical trap whose instantaneous center position is controlled by steering the focused optical beam.

When Eq. (1) describes the Brownian motion of a particle in an oscillating potential, the parameters have the following physical meaning: $C=k/\gamma$, where k is the stiffness of the trap, γ is the friction coefficient of the particle, $D=\sqrt{2k_BT/\gamma}$, $k_B=1.3807\times10^{-23}$ J/K is the Boltzmann constant, $\gamma=6\pi r\eta$ is the friction coefficient of the particle, r is the radius of the particle, η is the viscous coefficient of the liquid, and T is the absolute temperature of the system.

A. Experimental setup

The sample solution was prepared by adding a small amount of polystyrene beads (radius $r=295$ nm, Kisker-Biotech GmbH) to a 10% sodium dodecyl sulfate sterile aqueous solution. A drop (about 10 μl) of the resulting solution was placed between two coverslips (thickness 80 μm) separated by a 50-μm spacer and sealed with water-insoluble silicone vacuum grease to prevent evaporation. This sample was placed onto a custom-made sample holder on top of an inverted microscope equipped with an oil immersion microscope objective (100×, NA=1.25, Comar). The sample was illuminated from the top with a white light for visualization by a charge-coupled-device (CCD) camera. The particle concentration was sufficiently low to guarantee that there was only a single particle within the field of view. Three-dimensional nanometer positioning was achieved by a piezoelectric stage (Tritor 102, Piezosystem Jena) (see Fig. 3).

A single bead was trapped by focusing an optical beam with the objective near the upper coverslip surface in order to increase the drag force acting of the particle and therefore to have a more stable trapping. This optical beam was produced by a laser ($\lambda=785$ nm, maximum power 95 mW, MicroLaserSystem). Nanometer position detection was achieved using the forward-scattered light of a second beam, produced by a low-noise laser ($\lambda=635$ nm, maximum power 5 mW); its power at the sample was kept low in order that this beam does not affect the trapping of the probe. The forward scattering of the detection beam was collected by a condensator objective (40×, NA=0.75, UPlanFI) and projected onto a quadrant photodetector (QPD, New Focus 2911). The QPD measured the changes in the interferences pattern and converted them into three signals proportional to the position of the particle in the trap. These signals were sampled and acquired into a computer by an acquisition card (62621E, National Instruments). The sampling rate was $f_s=2$ kHz. This is sufficiently higher than the corner frequency of the system f_c and permits us to acquire the dynamics of the particle motion for the optical trap calibration [17]. In the study of the variance, since we are measuring the particle position distributions, we do not need to follow the dynamics of the particle. Therefore we can use a sampling rate that is much slower than the noise characteristic frequency.

The modulation of the position of the optical potential was achieved by an acousto-optical deflector/modulator (AOM/D ISOMET LS55 NIR). This was inserted along the 785-nm laser beam path and was used to steer it along the x direction. The y position of the trap was unaffected. The AOM/D input voltage was controlled by an arbitrary waveform generator (Tabor Electronics WW 5062) which allowed charging arbitrary signals. The power of the 785-nm beam before the objective was adjusted between 3 mW and 35 mW by the AOM/D.

B. Colored Gaussian noise generation

A noisy sequence with any PSD can be generated starting from a sequence of independent normally distributed random variables $\zeta_{n\,\Delta T}$—i.e., $\langle\zeta_{n\,\Delta T}\rangle=0$ and $\langle\zeta_{n\,\Delta T}\zeta_{(n+m)\Delta T}\rangle=\delta(m)$, where n and m are integers and ΔT is the sampling time. The most general approach involves (a) applying the Fourier transformation to the signal ζ_{nT}, (b) multiplying the resulting signal by a frequency-domain filter with the desired PSD, and (c) performing the inverse Fourier transformation of the resulting signal. The resulting signal has the desired PSD. A mathematically equivalent approach can be followed in the time domain by applying a time-domain filter. To generate the colored Gaussian noise, we used a finite-impulse-response (FIR) filter of the first order:

$$x_{0,(n+1)\Delta T}=\alpha x_{0,n\Delta T}+A/\sqrt{1-\alpha^2}\,\zeta_{(n+1)\Delta T}, \tag{8}$$

where A is the variance of $x_{0,n\Delta T}$ and α is its autocorrelation. This filter produces a low-pass signal whose cutoff frequency depends on the value of T and α: $f_0=-\ln\alpha/\Delta T$.

C. Data analysis

First for each value of the trapping power a series of data was acquired in the absence of modulation with a sampling rate $f_s=2$ kHz. The stiffness of the optical trap was measured in the x and y directions using the autocorrelation func-

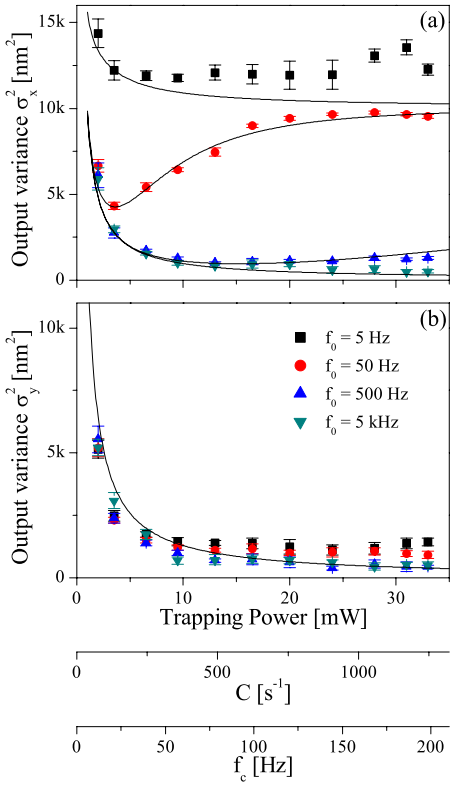

FIG. 4. (Color online) (a) Experimental and theoretical σ_x^2 as a function of the laser power in the presence of harmonic modulation of the trap center. From the bottom to the top the various sets of values correspond to f_0=5, 50, 500, 5000 Hz. The bar represents one standard deviation. The solid lines represent the theoretical prediction for the experimental parameters (k=0.4 pN/μm mW $\times$trapping power [mW], γ=1.1$\times 10^{-8}$ Ns/m, A=100 nm). The disagreement between experimental data and theoretical results for the right end of the 5-Hz data set is observed because for such values of the confinement effort and intrinsic noise frequency the trapping potential is not harmonic anymore. (b) Data for the nonmodulated direction y. The two additional axes show the value of the confinement effort and the corresponding cutoff frequency of the intrinsic noise.

tion method [17]. Furthermore, we have verified that no cross correlation between the two directions exists, which shows that the modulation does not introduce a rotational force field and that the results along the y direction are independent from the data along the x direction [17,18]. The values of the stiffness constant were found to be linear with the trapping optical power: $k_x \approx k_y$. In the calibration process the value of the friction coefficient of the particle γ takes into account the correction of the viscosity coefficient due to the proximity of the surface [19].

For each data point in Figs. 4–6 (see below), 12 data sets of 10 000 samples were acquired with a sampling rate f_s =2 kHz. The values of the output variances σ_x^2 and σ_y^2 are the average over these data sets. The error bars were calculated as the standard deviation of the measurements.

IV. EXPERIMENTAL RESULTS

Figure 4(a) illustrates the experimental results obtained with sinusoidal modulation of the trap center: $x_0(t)$ $=\sqrt{2}A\sin(2\pi f_0 t)$ with A=100 nm and f_0=5, 50, 500, and 5000 Hz. The solid lines represent the theoretical prediction according to Eq. (5). The experimental results are in very good agreement with the theoretical predictions for the entire

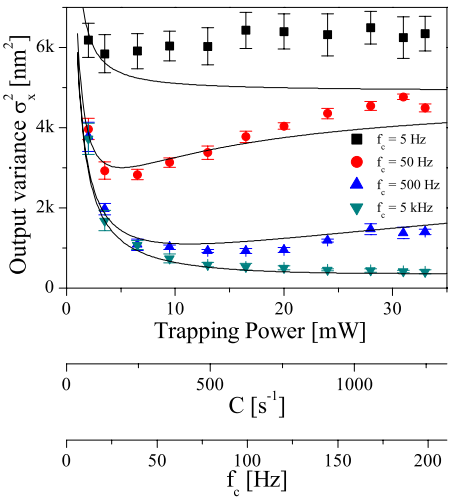

FIG. 5. (Color online) Experimental and theoretical σ_x^2 as a function of the trapping power obtained with colored Gaussian forcing of the equilibrium position. Various sets of values are presented for f_0=5, 500, 50, 5 Hz. The bars represent one standard deviation. The solid lines represent the theoretical prediction for the experimental parameters (k=0.7 pN/μm mW$\times$trapping power [mW], γ=1.9$\times 10^{-8}$ Ns/m, A=70 nm). The disagreement between experimental data and theoretical results for the right end of the 5-Hz data set is observed because for such values of the confinement effort and intrinsic noise frequency the trapping potential is not harmonic anymore. The two additional axes show the value of the confinement effort and the corresponding cutoff frequency of the intrinsic noise.

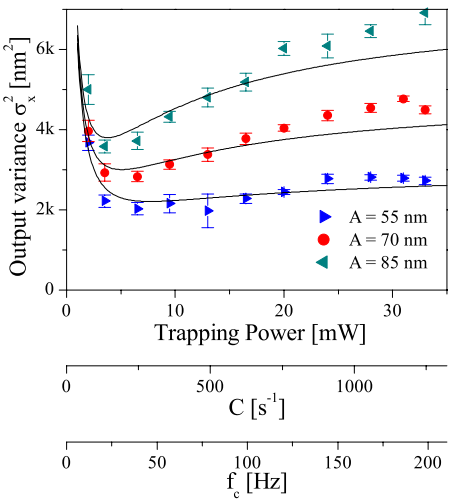

FIG. 6. (Color online) Experimental σ_x^2 as a function of the noise amplitude. Various sets of values are presented for A=55 70, 85 nm. The bars represent one standard deviation. The solid lines represent the theoretical prediction for the experimental parameters (k=0.7 pN/μm mW$\times$ trapping power [mW], γ=1.9 $\times 10^{-8}$ Ns/m). The two additional axes show the value of the confinement effort and the corresponding cutoff frequency of the intrinsic noise.

range of the trapping power, except for very low values. The maximal value of the dip at the dependence was found at the modulation frequency $f_0=50$ Hz at the confinement effort of $C=300$ s^{-1} when the corner frequency of the intrinsic noise of the system is $f_c=60$ Hz. As for the theoretical results, the modulation frequency to observe the stochastic resonant damping is higher than f_c. Hence, the stochastic resonant damping has a measurable value when the external source of modulation induced the movement of the probe with frequencies that are not present in the spectrum of the unmodulated internal motion.

To understand what physical quantities produce such a phenomenon, we can give an intuitive picture of the situation. When there is *stochastic resonant damping* in an overdamped system, the frequency of the intrinsic noise is such that in the time it takes the center of the trapping potential to move from one side to the other the particle has time to follow it only partially. Again this picture makes it clear that stochastic resonant damping, such as stochastic resonance, is not a real resonance, but only a pseudoresonance.

The trap was modulated only along the x direction, and the y movement of the particle was used to monitor for the same experimental condition the behavior of the system in the presence of only the *intrinsic noise*. As expected, the system variance σ_y^2 [Fig. 4(b)] increases with decreasing confinement effort and this behavior is independent from the modulation.

Figure 5(a) illustrates the experimental results for the correlated Gaussian modulation of the trap center. In this case the trap position moves as illustrated in the inset of Fig. 1(b) with $A=70$ nm and $f_0=5$, 50, 500, and 5000 Hz. There is very good agreement between the theoretical and experimental results. Again, as Fig. 5(b) shows, for the unmodulated direction the variance grows with decreasing confinement effort. Finally, in Fig. 6 the dependences of the confinement with the noise amplitude are presented for $A=55$, 70, and 85 nm. As was mentioned in the theoretical part, the stochastic resonant damping decreases with decreasing noise amplitude.

As can be seen in all the experimental figures, the agreement between experimental data and theoretical results gets worse for very low noise frequency and high confinement effort. For such parameters the optical trap cannot anymore be approximated as a harmonic potential; the system tends to become bistable, and Kramers transitions take place.

V. CONCLUSIONS

Usually in the presence of a background noise an increased effort put in controlling a system stabilizes its behavior. Rarely it is thought that an increased control of the system can lead to a looser response and, therefore, to a poorer performance. Strikingly there are many systems that show this weird behavior. Examples can be drawn form physical, biological [20], and social systems [21]. In scanning probe microscopy techniques, such as atomic force microscopy or photonic force microscopy, an increased control over the probe position does not necessarily improve resolution. In ecosystems the implementation of conservation policies can have unintended and perverse consequences [20]. Analogously, in social systems enforcement does not always achieve the desired effect, such as has been shown in ethnic and cultural conflicts [21] and economical systems [22,23]. We propose a simple and general mechanism underlying such behaviors: such a mechanism, named *stochastic resonant damping*, can be provided by the interplay between the background noise and the control exerted on the system.

ACKNOWLEDGMENTS

This research was carried out with the financial support of the Spanish Ministry of Education and Science (Grant No. NAN2004-09348). It was also partially supported by the Departament d'Universitats, Recerca i Societat de la Informació, and the European Social Fund.

[1] L. Gammaitoni, P. Hanggi, P. Jung, and F. Marchesoni, Rev. Mod. Phys. **70**, 223 (1998).
[2] R. D. Astumian, Science **276**, 917 (1997).
[3] C. R. Doering and J. C. Gadoua, Phys. Rev. Lett. **69**, 2318 (1992).
[4] C. Schmitt, B. Dybiec, H. Hanggi, and C. Bechinger, Europhys. Lett. **74**, 937 (2006).
[5] S. Leibler, Nature (London) **370**, 412 (1994).
[6] R. D. Astumian and M. Bier, Phys. Rev. Lett. **72**, 1766 (1994).
[7] J. M. G. Vilar and J. M. Rubi, Phys. Rev. Lett. **86**, 950 (2001).
[8] A. Gorlitz, M. Weidemuller, T. W. Hansch, and A. Hemmerich, Phys. Rev. Lett. **78**, 2096 (1997).
[9] G. Raithel, G. Birkl, A. Kastberg, W. D. Phillips, and S. L. Rolston, Phys. Rev. Lett. **78**, 630 (1997).
[10] R. Di Leonardo, G. Ruocco, J. Leach, M. J. Padgett, and A. J. Wright, Phys. Rev. Lett. **99**, 010601 (2007).
[11] Y. Deng, J. Bechhoefer, and N. R. Forde, J. Opt. A, Pure Appl. Opt. **9**, S256 (2007).
[12] Y. Seol, K. Visscher, and D. B. Walton, Phys. Rev. Lett. **93**, 160602 (2004).
[13] A. Manwani and C. Koch, Neural Comput. **13**, 1 (2001).
[14] S. M. Bezrukov and I. Vodyanov, Nature (London) **378**, 362 (1995).
[15] D. Nozaki, D. J. Mar, P. Grigg, and J. J. Collins, Phys. Rev. Lett. **82**, 2402 (1999).
[16] G. Mato, Phys. Rev. E **59**, 3339 (1999).
[17] G. Volpe, G. Volpe, and D. Petrov, Phys. Rev. E **76**, 061118 (2007).
[18] G. Volpe and D. Petrov, Phys. Rev. Lett. **97**, 210603 (2006).
[19] K. Berg-Sorensen and H. Flyvbjerg, Rev. Sci. Instrum. **75**, 594 (2004).
[20] J. Liu, T. Dietz, S. R. Carpenter, M. Alberti, C. Folke, E. Moran, A. N. Pell, P. Deadman, T. Kratz, J. Lubchenco,

E. Ostrom, Z. Ouyang, W. Provencher, C. L. Redman, S. H. Schneider, and W. W. Taylor, Science **317**, 1513 (2007).
[21] M. Lim, R. Metzler, and Y. Bar-Yam, Science **317**, 1540 (2007).
[22] R. N. Mantegna and H. E. Stanley, *An Introduction to Econophysics: Correlations and Complexity in Finance* (Cambridge University Press, Cambridge, England, 2000).
[23] W. M. Saslow, Am. J. Phys. **67**, 1239 (1999).